Femtosecond IR and UV laser induced periodic structures on steel and copper surfaces

Tauras Bukelis, Eugenijus Gaižauskas, Ona Balachninaitė *, Domas Paipulas

Vilnius University, Faculty of Physics, Laser Research Center, Saulėtekio Ave. 10, Vilnius, Lithuania

ARTICLE INFO

ABSTRACT

We analyze in detail laser induced periodic surface structures (LIPSS) on steel and copper surfaces. The chosen metals exhibit extreme differences between their thermal conductivity values, which determines the rate of extinguishing of the laser-induced temperature modulation on the surface. Two wavelengths of femtosecond laser radiation sources in IR and UV spectral range were used to inscribe low spatial frequency LIPSS. Regular LIPSS were successfully formed on steel samples for both wavelengths and it was observed that their regularity decreased with shorter wavelength used to induce the structures. For copper samples, LIPSS of considerably lower regularity were formed and even absent for one of the used scanning method at UV wavelength. Experimental results were analyzed in view of the numerical solution of the 2D heat diffusion equation for induced temperature on the surface. It was found that the temperature modulation decreased considerably faster (lasting tens of picoseconds) in copper, and (additionally) the decrease of the modulation is faster at the higher modulation frequency.

1. Introduction

Femtosecond laser processing of solid-state materials often results in the formation of laser-induced periodic surface structures (LIPSS). These patterns (also known as ripples, firstly revealed by Birnbaum [1] on semiconductor surface) become available on the surface of almost any material [2] and were regarded just as a 'side-effect' for a long time. However, studies of femtosecond LIPSS have received considerable attention over the last two decades due to the progress in ultra-short laser pulse generation and the plethora of technological applications for surface functionalization to control their optical, mechanical and chemical properties.

Owning to the exceptional large number of scientific papers on the matter we refer here to recently published reviews [3–9], where comprehensive state-of-the-art analysis is given. Nevertheless, it should be emphasized that even though there has been a large amount of theoretical and experimental work aimed at understanding LIPSS formation mechanisms and using this understanding to tailor surfaces for specific applications, the explanation of the formation of these periodic micro- and nano-structures is a more challenging task than the production of them. Indeed, as a well established fact of LIPSS formation mechanism the interference produced periodic distribution of laser energy during the excitation of the material should be stressed. Both the interference of the incoming and defect scattered light and the interference with surface plasmon-polariton (SPP) waves are responsible for this periodic

temperature modulation on the surface. The efficacy factor theory [10, 11], an electro-magnetic wave interference model to simulate the inhomogeneous energy deposition produced by the laser impinging at a rough surface, allows us to predict the formation of LIPSS depending on surface roughness and optical properties of the processed materials. But this and most of other existing models [12–18], as it was stressed by Gurevich [19], discuss only the appearance of a periodic modulation of the electron and ion temperatures and leaves unanswered the question: how the inhomogeneous surface temperature distribution induces the periodical structure on the surface.

Therefore, studies of the influence of specific material parameters on processes occurring after the formation of temperature modulation on the surface are extremely important. In recent papers [20] the context of ripple formation during laser materials processing involving melting of a surface by a laser beam was discussed hinting to the involvement of hydrodynamic processes in their origin. It was shown, particularly, that the ripple formation could be triggered by a periodical external force, e.g. by appropriate repetition rate of an incident laser beam.

It is also worth noting the findings given in [21] on the physical mechanisms governing LIPSS regularity. Here the possibilities of regular LIPSS formation were linked with the mean free path of the excited surface electromagnetic waves (SEW) in the group of transition metals. Owning to this parameter, high-regularity LIPSS (HR LIPSS)
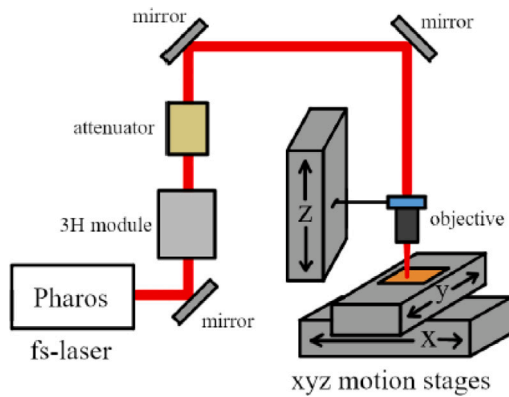
Fig. 1. Experimental setup for LIPSS formation.

Fig. 2. SEM images of an untreated steel and copper samples.

were obtained on Ti, Mo and steel. Conversely, in the rest of studied metals (Au, Cu and Al, possessing long mean free path values of the SEW), HR LIPSS were not observed. It should be pointed out that latter metals are characterized by exceptionally high thermal diffusivity, contrary to the above mentioned titanium, molybdenum and steel.

In this work we aim to investigate HR LIPSS formation on surfaces of steel and copper, possessing different (contrasting) heat conduction values. Specifically, we investigate LIPSS regularity dependencies on scanning method, overlap of laser beams and fluence using laser radiation in IR and UV spectral ranges.

2. Experimental setup and measurement methods

Laser induced periodic surface structure experiments were carried out on thick steel and copper samples of various surface qualities using femtosecond laser systems carrying IR and UV radiation at 1030 and 343 nm, respectively.

2.1. Radiation sources and experimental setup

The femtosecond ($\sim$ 300 fs) laser system (diode pumped femtosecond laser with an integrated oscillator and amplifier) used in this experiment was Pharos Yb:KGW laser (Light Conversion, Ltd. Lithuania) operating at 1030 nm wavelength, with the output of up to 6 W of the average power. Integrated pulse picker allowed pulse-on-demand operation and a variable repetition rate from single shot pulses to 1 MHz. For forming laser induced periodic surface structures, the repetition rate was fixed at 100 kHz, and the average output power was fixed at 630 mW. An additional attenuator consisting of a half-wave plate and a thin-film polarizer was used to vary the incident laser power on the sample. The laser beam diameter at the lens was calculated to be (7.5$\pm$ 0.8) mm using the scanning knife-edge method. Third harmonic generation module was used to achieve UV laser radiation at 343 nm with the maximum available average power of 200 mW. For LIPSS formation experiments the average UV laser power not exceeding 50 mW was chosen.

This system also was equipped with a f-theta lens, installed in the galvo-scanner assembly, which allows to focus the laser radiation down to beam spots d_{UV} = (7.5$\pm$ 0.8) μm and d_{IR} = (8.2$\pm$ 0.8) μm for UV and IR radiation, respectively. Note that for the IR radiation wavelength (λ = 1030 nm) focusing conditions satisfies one of the high regularity LIPSS formation requirements $d < 10\lambda$ [21]. XYZ motion stages were used for objective and beam positioning (see Fig. 1). For the experiments stainless steel (304S) and copper (Cu-OFHC; 99.95%) samples with the surface roughness Ra of (581$\pm$ 5) nm and (372$\pm$ 4) nm respectively were chosen. The surface roughness Ra (the arithmetic average of the absolute values of the roughness profile ordinates) was measured using optical profilometer "Sensofar PLμ 2300". SEM images of the untreated steel and copper samples are shown in Fig. 2.
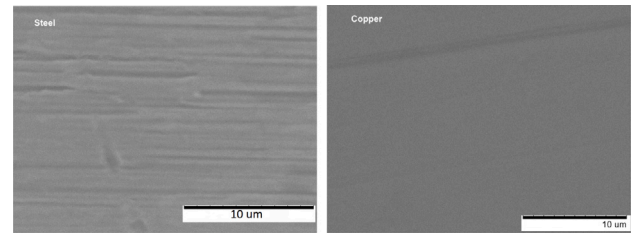
2.2. LIPSS regularity assessments

According to [21] LIPSS regularity could be characterized by the dispersion of LIPSS orientation angle (DLOA). If DLOA is less than 10 deg, the LIPSS is called highly regular (HR-LIPSS). A high-resolution images of fabricated structure were taken using a scanning electron microscope (SEM) as it is shown in Fig. 3. The image of the surface structure then was digitally processed by applying 2D Fourier transformation to extract the frequency and angle data. Distribution of LIPSS orientation angle graph was generated from a SEM image using freely available OrientationJ plugin [22] written for the ImageJ [23] open-source software. From a graph depicting the structure orientation distribution is then constructed in which a single peak can be seen if the LIPSS was produced using linearly polarized laser radiation. The peak width is evaluated at the half width at half maximum (HWHM), which corresponds to the DLOA value, as it is shown in the sketch of DLOA value evaluation (see Fig. 3). The regularity parameter R was evaluated as reciprocal of the DLOA value. It should be mentioned that such an evaluation method requires both surface imaging and digital processing, which make this approach rather slow. Moreover, the method does not take into consideration the depth of the ripples. Nevertheless, the regularity assessment is rather accurate and the surface structures can be further visually inspected. Further, to improve analysis of the quality of the DLOA, the surface roughness was removed from each LIPSS image. For this purpose, 2D-FFT was performed on every image to acquire the spatial frequency domain representation on which a mask was applied, followed by an inverse 2D-FFT to remove all low-frequency components. An example of the LIPSS image corrected by this procedure is shown in Fig. 4.

2.3. Experimental results of LIPSS formation on the metal surfaces

For each sample of copper and steel, at least two tables of arrays of LIPSS formation results were built in our experiment, using mentioned laser systems possessing wavelengths in IR and UV regions. Each array consisted of a grid of laser-treated areas where each row had a constant fluence while constant beam overlap was characteristic for columns. All LIPSS have been formed using a constant polarization direction perpendicular to the scanning direction. After forming some trial LIPSS arrays on different samples it was noticed that higher quality LIPSS tend to form on samples with a polished surface, therefore, copper and steel samples were polished to increase the surface smoothness (RMS values were 482 nm and 755 nm for copper and steel, respectively). For the LIPSS formation on areas of metals two scanning methods were used: (a) forming parallel lines from densely packed laser beams (scanning direction overlap from 98.2–99.9%) and line overlap between lines from 73 to 80% overlap); (b) keeping constant distance between beams in the scanning direction and between each scanned line with constant (from 30 to 80%) overlap, as illustrated in Fig. 5. Different scanning methods were chosen in order to analyze their influence on the formed LIPSS regularity.
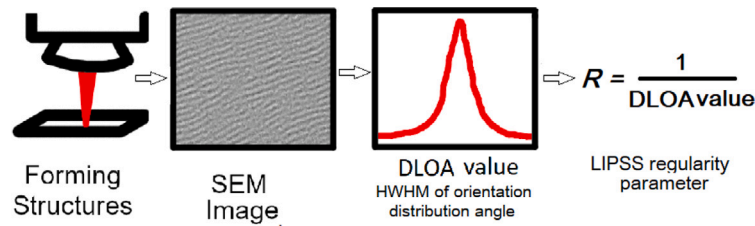
Fig. 3. Sketch of evaluation steps of the regularity parameter R from SEM image of LIPSS.
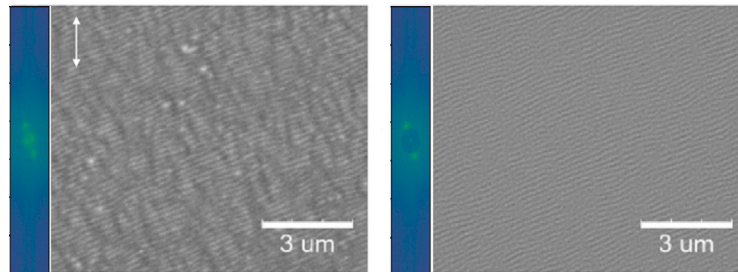

Fig. 4. An example of a LIPSS SEM image before and after surface roughness removal using 2D-FFT (shown on the left for each image) masking. White arrow indicates the polarization of laser light.
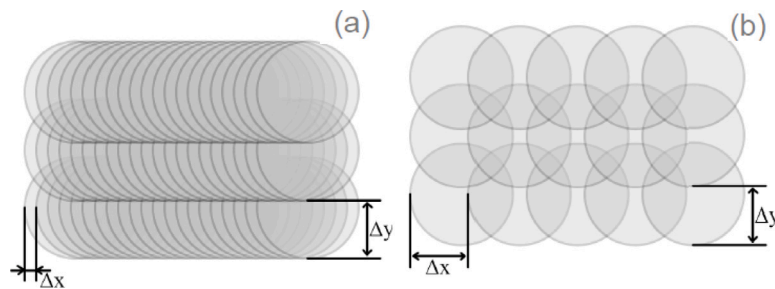

Fig. 5. Illustrations for scanning methods used in experiments: (a) - dense lines scanning; (b) - scanning using constant beam overlap.

2.3.1. LIPSS formation with dense lines scanning method

Here we present results of LIPSS arrays experimentally formed using dense lines scanning method on the steel and copper samples, irradiated by IR and UV laser pulses. The chosen polarization was perpendicular to the scanning direction and controlled using a half-wave plate. The fluences used in this system were varied between 0.11 J/cm^2 and 0.21 J/cm^2 for steel and between 0.45 J/cm^2 and 0.61 J/cm^2 for copper, while the scanning speed was varied between 0.5 mm/s to 3 mm/s for both materials. SEM images of the LIPSS areas were taken and from those images the LIPSS regularity parameter R was evaluated. The LIPSS images of the highest regularity on each of the metals are shown in Fig. 6 (top) .

LIPSS were successfully formed in the most of the arrays cells on the steel samples using IR laser pulses. A trend of increasing LIPSS regularity with increasing both scan speed and fluence was observed from the values. The highest LIPSS regularities were achieved on a polished steel sample at 3.0 mm/s scan speed in a wide range (from 0.13 to 0.19 J/cm^2) of fluences. For copper the regularity in this case was lower and it was achieved at lower scan speeds and higher fluence. The same trend (increased LIPSS regularity with increasing both the scan speed and the fluence) as for steel samples should be noticed. Images of these surface structures as well as the combined colormap of R values can be seen in Fig. 6 (bottom row).

LIPSS formation results using UV radiation differ from the described above. Considerably increased fluences for regular LIPSS formation on the steel and copper samples are required for UV radiation, compared to IR. The highest LIPSS regularity in this case ($R = 0.12$) was achieved both on steel and copper samples at 3.0 mm/s scan speed, using 0.7 J/cm^2 and 2.4 J/cm^2 fluences, respectively. Images of formed surface structures as well as color-maps of R values for this case are shown in Fig. 7.

2.3.2. LIPSS formation with constant beam overlap

As for the LIPSS formation method keeping the constant distance in both scan directions, the significantly lower beam overlap and as a result, the higher radiation fluence required to form a regular LIPSS should be emphasized. As it is seen from Fig. 8 in this scanning configuration the best regularity (overall in our experiments) result ($R = 0.25$) was obtained in steel using IR laser at fluence as high as 3.0J/cm^2 and beam overlap of 70%. To form highly regular LIPSS in copper using the same scanning configuration was rather challenging task and the result was considerable worse ($R = 0.075$), obtained for the same fluence and slightly higher overlap (80%). Finally, using UV laser irradiation we do not succeed to form any LIPSS in copper, and rather pure regularity was achieved for steel samples at extremely high 30 J/cm^2 fluence and the highest 80% overlap, used in our experiments (see Fig. 9). The periods of the formed LIPSS by using IR laser irradiation were a bit smaller than used laser wavelength and equal to 0.85 µm and 0.95 µm for steel and copper respectively. LIPSS formed using UV laser irradiation had the periodicity of 0.18 µm and 0.22 µm for steel and copper respectively.

In summarizing the experimental results, two things should be highlighted. First, in both scanning configurations, higher values of LIPS
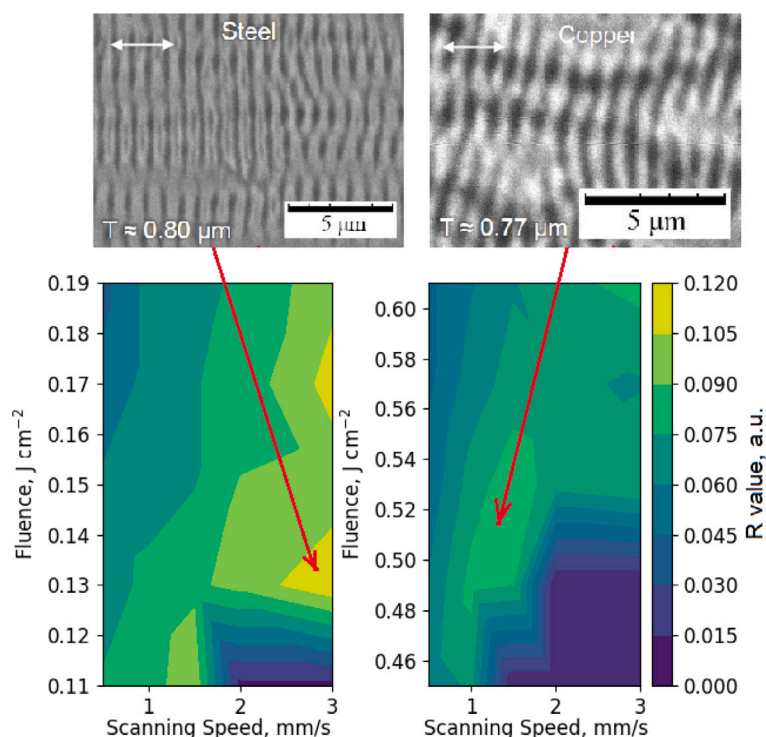
Fig. 6. LIPSS images (top row) and colormaps of R values (bottom row) for steel and copper obtained using IR laser radiation. White arrows indicate the polarization of laser light. (For interpretation of the references to color in this figure legend, the reader is referred to the web version of this article.)

Fig. 7. LIPSS images (top) and color-maps of R values with combined color-bar (bottom) for steel and copper obtained using UV laser radiation. White arrows indicate the polarization of laser light. (For interpretation of the references to color in this figure legend, the reader is referred to the web version of this article.)
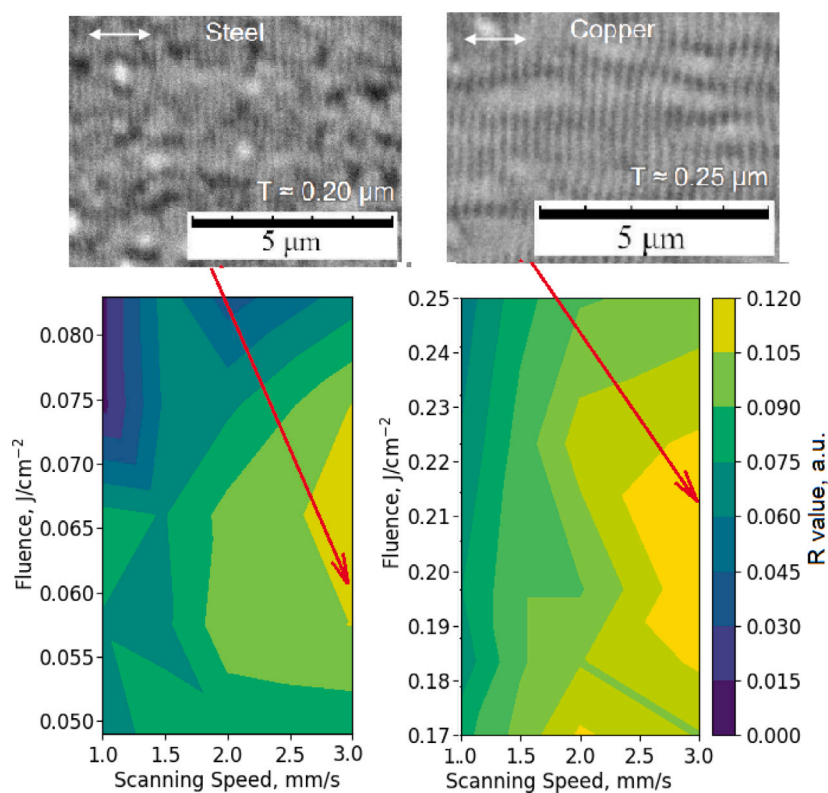
regularity R were observed for steel. Secondly, reducing the focusing beam spot area using UV radiation failed to improve the value of the LIPSS regularity R for steel and LIPSS was not observed in this region for copper. On the other hand, in the mentioned above paper [21], owning to the shorter mean free path of SEW excited by blue or near-UV laser light, was predicted dramatically improved the possibility of the
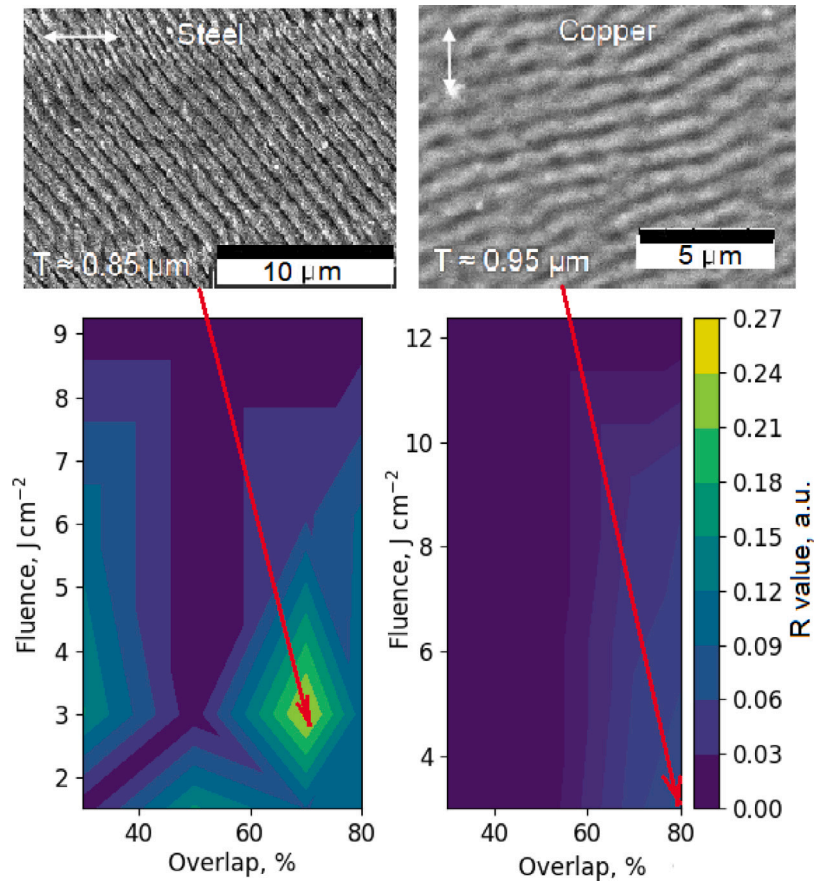
Fig. 8. LIPSS images inscribed on steel and copper surfaces by constant overlap of IR laser beams (top). Colormaps of LIPSS regularity values R are shown in the bottom for steel and copper samples, respectively. White arrows indicate the polarization of laser light. (For interpretation of the references to color in this figure legend, the reader is referred to the web version of this article.)

Fig. 9. Highest regularity LIPSS image inscribed on steel surface using UV laser pulses and constant overlap scanning method (left). Colormap of the regularity values for this case (right). White arrow indicates the polarization of laser light. (For interpretation of the references to color in this figure legend, the reader is referred to the web version of this article.)
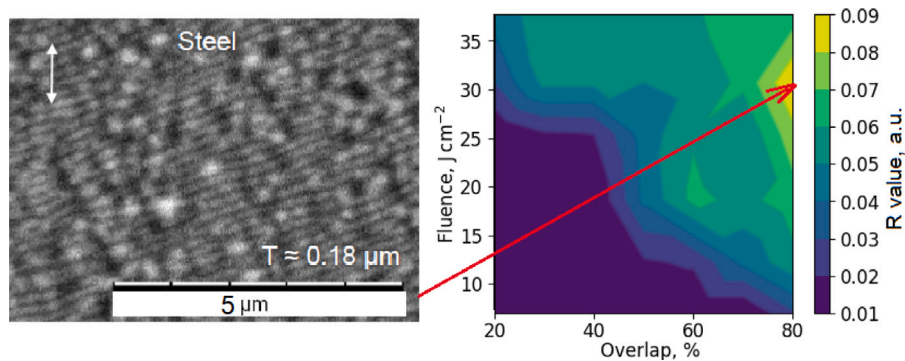
regular LIPSS for many metals, including copper. However, it should be stressed that this statement is true at a fixed temperature modulation rate.

3. Discussions

An ultrafast photoexcited metal on the time scale of several picoseconds evolves towards an electronic thermalized system, heating initially cold lattice. As it was mentioned in the introduction, it is well established that material, namely the electron system, is excited periodically due to the interference of the incoming and SEW waves. This excitation results in the spatial temperature modulation of the surface and due

to the electron–phonon interaction energy is transferred to the lattice, giving rise to a number of complex physical processes (e.g. melting, evaporation, and resolidification) to develop in the overheated lattice.

During surface resolidification, depending on the excitation conditions, the instantaneous temperature-induced morphology can be preserved in the form of LIPSS. Note that compared to lattice heating the reorganization of matter takes place on a significantly longer, typically tens of picoseconds (and even longer) time scale [24]. The general trends of the initial stages of the lattice heating dynamics were carefully analyzed using a two-temperature model (TTM) [25] in many papers, where the significant impact of electron–phonon coupling was

stressed. To be mentioned here is the numerical study of periodic surface structure formation on noble metals (Cu, Al, and Au) [26], where a greater electron-lattice coupling coefficient was found beneficial for more pronounced LIPSS structure formation in metals possessing similar thermal and transport parameters. The spatiotemporal evolution of modulation of laser energy coupling with two different materials, a metal (Ti) and a semiconductor (Si) was investigated in paper [27]. The simulation results show that even for moderate laser fluence (when the minimum of induced temperature appears close to the melting point) modulation of the lattice temperature is not smoothened before thermalization between the electron and lattice subsystems. The thermal modulation can exist at about 10 ps after the pulse action for titanium and more than 50 ps for silicon. Regarding the formation of LIPSS on steel and copper surfaces, two more works [28,29] are noteworthy. However, theoretical investigations here are conducted under the assumption of strong excitation conditions, sufficient to induce mass removal (ablation), melting, and evaporation of a portion of the material.

As temperature modulation plays a crucial role in the formation of LIPSS, it makes sense to evaluate the influence of heat diffusion on changes in the depth of spatial temperature modulation in steel and copper, since the rate of heat diffusion in these metals differs dozens of times.

3.1. Numerical analysis of the ultrashort pulse induced temperature modulation dynamics on the overheated surface

In this subsection we provide results of numerical analysis of the temperature modulation changes, dominated due to heat diffusion in the steel and copper samples, using Python package $py - pde$ [30]. Our analysis is focused on the time scale starting with the end of the laser pulse and lattice heating, so that both source and electron–phonon interaction terms vanishes in two-temperature equations [25]. In fact, we start with the third step in recently proposed [31,32] three-step LIPSS formation description, which constitute of: (I) modulation of the electron temperature, (II) imprinting periodic modulation on the lattice, and (III) temperature modulation induced relocation of the material. Specifically, we consider time dependency of the temperature distribution $T(x, z, t)$ in the steel and copper samples by solving 2D diffusion equation of the following form:

$$\frac{\partial T(x, z, t)}{\partial t} = D\nabla_{\perp}^2 T(x, z, t). \tag{1}$$

We assume that upon femtosecond laser irradiation both metals experience modulated spatial melting on their surface, and near melting-threshold fluences will be applied. According to evaluation made in [17,18,27] lattice temperature modulation depth T_{mod} approaches 1000 ° C in metals. Therefore, it is reasonable to write the initial condition for temperature distribution in the following form:

$$T(x, y, 0) = T_0 + T_{mod}\left[1 + \exp(-\alpha z)\cos^2\left(\frac{k_\lambda}{2}x\right)\right]. \tag{2}$$

Here $T_0 = 300$ K is taken for the sample at room temperature and $T_{mod} = 800$ K, noting that for used T_0 and T_{mod} values the sample becomes overheated initially to 1900K at oscillation maxima and exceeds that melting temperatures, which are 1510K and 1084K for stainless steel and copper, respectively. Wavenumber $k_\lambda = 2\pi/\lambda$ specifies the modulation frequency created due to interference of laser radiation and SEW for the wavelengths of the IR and UV lasers and absorption constant $\alpha = 10/\lambda$ μm^{-1} was taken as an approximation value for the ballistic electron movement distance in metals. Note that we have reduced the 3D problem into 2D by taking into account that the laser spot size was much larger compared to the period of temperature modulation.

Eq. (1) was solved numerically considering periodic boundary conditions along surface coordinate x, as well as the Neumann boundary condition along the beam propagation coordinate z, taking zero derivatives for temperature function on the end face of the sample. Heat flux through the front face (heat convection on the metal–air interface) was disregarded and diffusion constant D was set to 111 and 3 (nm^2 ps^{-1}) for steel and copper, respectively.

Results of the modeling for IR and UV laser initiated temperature modulation in the material under investigation taking dimensions of the samples as large as 5 μm x 0.5 μm are shown in Figs. 10 and 11. As it is seen from modeling results at 50ps after excitation steel samples still preserve deep temperature modulation. Even if the melting point was exceeded initially for both (1030 nm and 343 nm) laser wavelengths, the copper samples' situation differs to a very great degree. Here, considerably less modulation can be seen preserved for the excitation at 1030 nm, but for the excitation using UV laser at 343 nm wavelength temperature modulation in copper becomes vanishing after 50ps.

3.2. The influence of heat diffusion on the LIPSS formation possibility

Let us note that the model used above is simplified in that it did not include any of the processes that occur after instantaneous raising temperature above the melting point, such as melting, vaporization (ablation), and resolidification. Even more, we understand the ongoing processes start in the absence of thermodynamic equilibrium when the state cannot be characterized by the temperature. Nevertheless, provided above comparative LIPSS formation study on copper and steel surfaces allows one to assume that metals possessing lower heat diffusion rates are advantageous for formation of LIPSS with higher regularity. Indeed, looking at the above-presented experimental results and taking into account the modeling of thermal diffusion in steel and copper, the following things could be noticed. Firstly, the higher diffusion rate requires considerably higher field fluence to form a high regularity LIPSS for the same scanning conditions. And considerably better results (higher regularity of LIPSS) are obtained in the steel, characterized by a lower rate of heat diffusion. Secondly, thermal diffusion has a more significant influence on the formation of regular LIPSS in the region of shorter wavelengths, since its transverse component (along the lateral coordinate x) has a greater influence in suppressing the temperature modulation depth for higher spatial frequencies.

Need to emphasize that this observation in the case of forming structures using the dense scanning method (see Figs. 6 and 7) is not of great significance and could be explained by the better feedback and accumulation effects from the previous sequence of shots in this scanning configuration. On the other hand, it can be seen from the results obtained using constant overlap scanning (see Fig. 8) that the structures formed in the IR region are of significantly lower quality in copper than those in steel. And what is more, using the UV radiation and the constant overlap scanning method we did not succeed in forming HR LIPSS for UV wavelength at all.

4. Conclusions

In this study we investigated low spatial frequency LIPSS induced on copper and steel by femtosecond laser beams in UV and IR wavelength ranges. Due to the shorter free path of the excited SEW, LIPSS formation using shorter laser wavelengths hints at higher regularity for some metals (like copper, gold, silver, aluminum, etc.) [21]. Nevertheless, there are more conditions that need to be tuned in order for HR LIPSS to be obtained. One of such parameter is heat conductivity, which allows forming LIPSS of higher regularity in steel as compared to copper, characterized by considerably greater heat conductivity. The scanning method also greatly affects LIPSS formation, hinting that there might be some accumulative effects that allow LIPSS to form on metals like copper. Higher LIPSS regularity was observed at fluences near the LIPSS formation threshold for IR wavelengths.
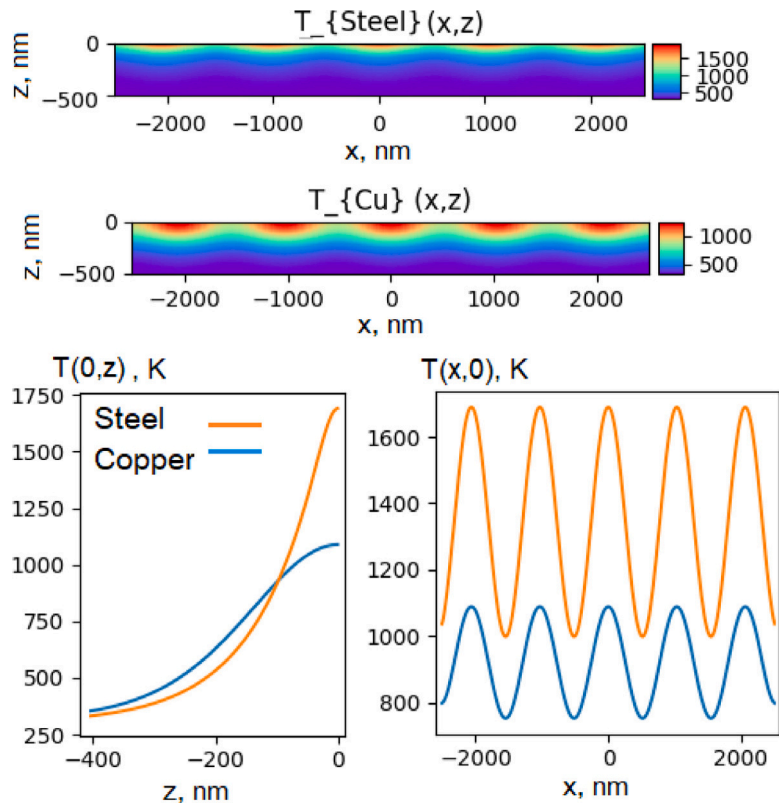
Fig. 10. Images of temperature profiles at 50 ps after the IR radiation ($\lambda = 1030$ nm) induced modulated thermal load for steel and copper (top rows), and slices of temperature modulation along the *x* and *z* coordinates (bottom row). (For interpretation of the references to color in this figure legend, the reader is referred to the web version of this article.)

Fig. 11. Images of temperature profiles at 50ps after the initially UV laser ($\lambda = 343$ nm) induced modulated thermal load (top rows), and slices of temperature modulation along the *x* and *z* coordinates (bottom row). (For interpretation of the references to color in this figure legend, the reader is referred to the web version of this article.)
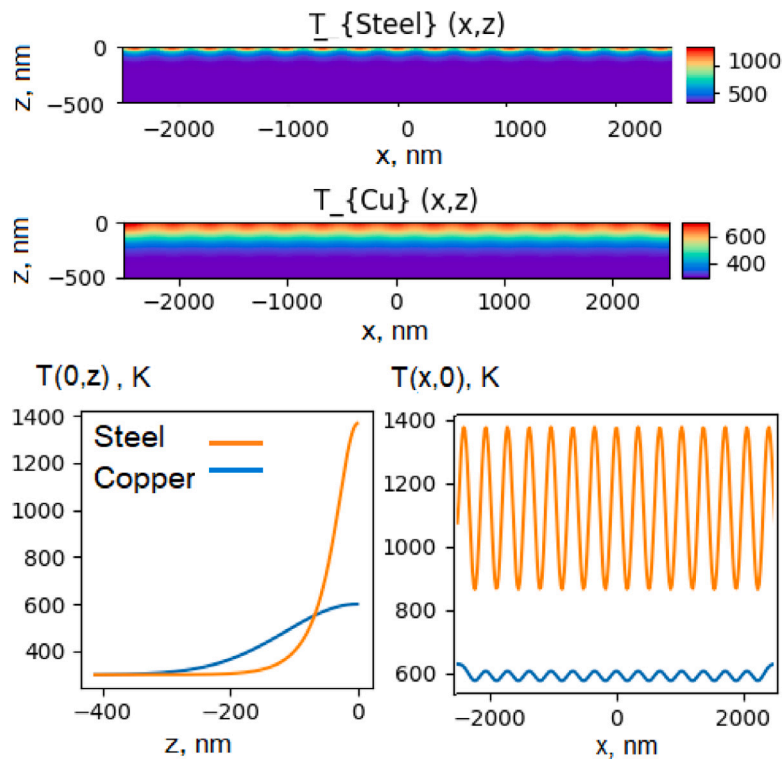
CRediT authorship contribution statement

Tauras Bukelis: Investigation, Methodology, Writing – original draft. **Eugenijus Gaižauskas:** Software, Validation, Formal analysis, Writing – original draft. **Ona Balachninaitė:** Conceptualization, Methodology, Writing – original draft. **Domas Paipulas:** Writing – review & editing, Conceptualization, Funding acquisition.

Declaration of competing interest

The authors declare the following financial interests/personal relationships which may be considered as potential competing interests: Domas Paipulas reports financial support was provided by Research Council of Lithuania.

Data availability

Data will be made available on request.

Acknowledgments

Appendix A. Supplementary data

Supplementary material related to this article can be found online at https://doi.org/10.1016/j.surfin.2023.102869.

References

[1] Milton Birnbaum, Semiconductor surface damage produced by ruby lasers, J. Appl. Phys. 36 (1965) 3688–3689, http://dx.doi.org/10.1063/1.1703071.

[2] H.M. van Driel, J.E. Sipe, Jeff F. Young, Laser-induced periodic surface structure on solids: A universal phenomenon, Phys. Rev. Lett. 49 (1982) 1955–1958, http://dx.doi.org/10.1103/PhysRevLett.49.1955, URL https://link.aps.org/doi/10.1103/PhysRevLett.49.1955.

[3] Ričardas Buividas, Mindaugas Mikutis, Saulius Juodkazis, Surface and bulk structuring of materials by ripples with long and short laser pulses: Recent advances, Progr. Quantum Electron. 38 (3) (2014) 119–156, http://dx.doi.org/10.1016/j.pquantelec.2014.03.002, URL https://www.sciencedirect.com/science/article/pii/S0079672714000044.

[4] Mario Garcia-Lechuga, Daniel Puerto, Yasser Fuentes-Edfuf, Javier Solis, Jan Siegel, Ultrafast moving-spot microscopy: Birth and growth of laser-induced periodic surface structures, ACS Photonics 3 (10) (2016) 1961–1967, http://dx.doi.org/10.1021/acsphotonics.6b00514.

[5] Jörn Bonse, Sandra Höhm, Sabrina V. Kirner, Arkadi Rosenfeld, Jörg Krüger, Laser-induced periodic surface structures— A scientific evergreen, IEEE J. Sel. Top. Quantum Electron. 23 (3) (2017) http://dx.doi.org/10.1109/JSTQE.2016.2614183.

[6] Jörn Bonse, Quo vadis LIPSS?—Recent and future trends on laser-induced periodic surface structures, Nanomaterials 10 (10) (2020) 1950, http://dx.doi.org/10.3390/nano10101950.

[7] Jörn Bonse, Stephan Gräf, Maxwell meets marangoni—A review of theories on laser-induced periodic surface structures, Laser Photonics Rev. 14 (10) (2020) 2000215, http://dx.doi.org/10.1002/lpor.202000215, arXiv:https://onlinelibrary.wiley.com/doi/pdf/10.1002/lpor.202000215.

[8] Stephan Gräf, Formation of laser-induced periodic surface structures on different materials: fundamentals, properties and applications, Adv. Opt. Technol. 9 (1–2) (2020) 11–39, http://dx.doi.org/10.1515/aot-2019-0062.

[9] Xiaofeng Xu, Laifei Cheng, Xiaojiao Zhao, Jing Wang, Xinyi Chen, Micro/nano periodic surface structures and performance of stainless steel machined using femtosecond lasers, Micromachines 13 (6) (2022) http://dx.doi.org/10.3390/mi13060976, URL https://www.mdpi.com/2072-666X/13/6/976.

[10] J.E. Sipe, Jeff F. Young, J.S. Preston, H.M. van Driel, Laser-induced periodic surface structure. I. Theory, Phys. Rev. B 27 (2) (1983) 1141–1154, http://dx.doi.org/10.1103/PhysRevB.27.1141.

[11] Rosenfeld Arkadi Bonse Joern, Krueger Joerg, On the role of surface plasmon polaritons in the formation of laser-induced periodic surface structures upon irradiation of silicon by femtosecond-laser pulses, J. Appl. Phys. 106 (2009) 104910, http://dx.doi.org/10.1063/1.3261734.

[12] SA Akhmanov, Vladimir I Emel'yanov, Nikolai I Koroteev, VN Seminogov, Interaction of powerful laser radiation with the surfaces of semiconductors and metals: nonlinear optical effects and nonlinear optical diagnostics, Soviet Phys. Uspekhi 28 (12) (1985) 1084–1124, http://dx.doi.org/10.1070/pu1985v028n12abeh003986.

[13] D. Dufft, A. Rosenfeld, S.K. Das, R. Grunwald, J. Bonse, Femtosecond laser-induced periodic surface structures revisited: A comparative study on ZnO, J. Appl. Phys. 105 (3) (2009) http://dx.doi.org/10.1063/1.3074106, URL https://www.osti.gov/biblio/21186020.

[14] Juergen Reif, Olga Varlamova, Sergej Varlamov, Michael Bestehorn, The role of asymmetric excitation in self-organized nanostructure formation upon femtosecond laser ablation, Appl. Phys. A 104 (3) (2011) 969–973, http://dx.doi.org/10.1007/s00339-011-6472-3.

[15] Juergen Reif, Olga Varlamova, Sebastian Uhlig, Sergej Varlamov, Michael Bestehorn, On the physics of self-organized nanostructure formation upon femtosecond laser ablation, Appl. Phys. A 117 (1) (2014) 179–184, http://dx.doi.org/10.1007/s00339-014-8339-x.

[16] J.P. Colombier, Florence Garrelie, Nicolas Faure, Stéphanie Reynaud, Mourad Bounhalli, Éric Audouard, Razvan Stoian, Florent Pigeon, Effects of electron-phonon coupling and electron diffusion on ripples growth on ultrafast-laser-irradiated metals, J. Appl. Phys. 111 (2012) 024902.

[17] P.N. Terekhin, O. Benhayoun, S.T. Weber, D.S. Ivanov, M.E. Garcia, B. Rethfeld, Influence of surface plasmon polaritons on laser energy absorption and structuring of surfaces, Appl. Surf. Sci. 512 (2020) 144420, http://dx.doi.org/10.1016/j.apsusc.2019.144420, URL https://www.sciencedirect.com/science/article/pii/S0169433219332362.

[18] O. Benhayoun, P.N. Terekhin, D.S. Ivanov, B. Rethfeld, M.E. Garcia, Theory for heating of metals assisted by surface plasmon polaritons, Appl. Surf. Sci. 569 (2021) 150427, http://dx.doi.org/10.1016/j.apsusc.2021.150427, URL https://www.sciencedirect.com/science/article/pii/S0169433221015014.

[19] Evgeny L. Gurevich, Mechanisms of femtosecond LIPSS formation induced by periodic surface temperature modulation, Appl. Surf. Sci. 374 (2016) 56–60, http://dx.doi.org/10.1016/j.apsusc.2015.09.091, URL https://www.sciencedirect.com/science/article/pii/S0169433215021856 E-MRS 2015 Spring Meeting Symposium CC: "Laser and plasma processing for advanced applications in material science", 11-15 May 2015, Lille (France).

[20] Klaus Morawetz, Sarah Trinschek, Evgeny L. Gurevich, Interplay of viscosity and surface tension for ripple formation by laser melting, Phys. Rev. B (2022).

[21] Iaroslav Gnilitskyi, Thibault J.-Y. Derrien, Yoann Levy, Nadezhda M. Bulgakova, Tomáš Mocek, Leonardo Orazi, High-speed manufacturing of highly regular femtosecond laser-induced periodic surface structures: physical origin of regularity, Sci. Rep. 7 (1) (2017).

[22] Zsuzsanna Püspöki, Martin Storath, Daniel Sage, Michael Unser, Transforms and operators for directional bioimage analysis: A survey, in: Winnok H. De Vos, Sebastian Munck, Jean-Pierre Timmermans (Eds.), Focus on Bio-Image Informatics, Springer International Publishing, Cham, 2016, pp. 69–93, http://dx.doi.org/10.1007/978-3-319-28549-8_3.

[23] Johannes Schindelin, Curtis T. Rueden, Mark C. Hiner, Kevin W. Eliceiri, The imagej ecosystem: An open platform for biomedical image analysis, Molecular Reproduct. Dev. 82 (7–8) (2015) 518–529, http://dx.doi.org/10.1002/mrd.22489, arXiv:https://onlinelibrary.wiley.com/doi/pdf/10.1002/mrd.22489.

[24] Pavel N. Terekhin, Jens Oltmanns, Andreas Blumenstein, Dmitry S. Ivanov, Frederick Kleinwort, Martin E. Garcia, Baerbel Rethfeld, Jürgen Ihlemann, Peter Simon, Key role of surface plasmon polaritons in generation of periodic surface structures following single-pulse laser irradiation of a gold step edge, Nanophotonics 11 (2) (2022) 359–367, http://dx.doi.org/10.1515/nanoph-2021-0547.

[25] Sergei I. Anisimov, B.L. Kapeliovich, T.L. Perelman, Electron emission from metal surfaces exposed to ultrashort laser pulses, J. Exp. Theor. Phys. (1974).

[26] Wang Jincheng, Guo Chunlei, Numerical study of ultrafast dynamics of femtosecond laser-induced periodic surface structure formation on noble metals, J. Appl. Phys. 102 (2007) 053522, http://dx.doi.org/10.1063/1.2776004.

[27] Yoann Levy, Thibault J.-Y. Derrien, Nadezhda M. Bulgakova, Evgeny L. Gurevich, Tomáš Mocek, Relaxation dynamics of femtosecond-laser-induced temperature modulation on the surfaces of metals and semiconductors, Appl. Surf. Sci. 374 (2016) 157–164, http://dx.doi.org/10.1016/j.apsusc.2015.10.159, URL https://www.sciencedirect.com/science/article/pii/S0169433215025787 E-MRS 2015 Spring Meeting Symposium CC: "Laser and plasma processing for advanced applications in material science", 11-15 May 2015, Lille (France).

[28] George D. Tsibidis, Alexandros Mimidis, Evangelos Skoulas, Sabrina V. Kirner, Jörg Krüger, Jörn Bonse, Emmanuel Stratakis, Modelling periodic structure formation on 100cr6 steel after irradiation with femtosecond-pulsed laser beams, Appl. Phys. A 124 (1) (2017) 27, http://dx.doi.org/10.1007/s00339-017-1443-y.

[29] Chin Lun Chang, Chung-Wei Cheng, Jinn Kuen Chen, Femtosecond laser-induced periodic surface structures of copper: Experimental and modeling comparison, Appl. Surf. Sci. 469 (2019) 904–910, http://dx.doi.org/10.1016/j.apsusc.2018.11.059.

[30] David Zwicker, py-pde: A Python package for solving partial differential equations, J. Open Sour. Softw. 5 (48) (2020) 2158, http://dx.doi.org/10.21105/joss.02158.

[31] Stella Maragkaki, Thibault J.-Y. Derrien, Yoann Levy, Nadezhda M. Bulgakova, Andreas Ostendorf, Evgeny L. Gurevich, Wavelength dependence of picosecond laser-induced periodic surface structures on copper, Appl. Surf. Sci. 417 (2017) 88–92, http://dx.doi.org/10.1016/j.apsusc.2017.02.068, URL https://www.sciencedirect.com/science/article/pii/S0169433217304191 10th International Conference on Photoexcited Processes and Applications.

[32] Evgeny L. Gurevich, Yoann Levy, Nadezhda M. Bulgakova, Three-step description of single-pulse formation of laser-induced periodic surface structures on metals, Nanomaterials 10 (2020) http://dx.doi.org/10.3390/nano10091836.